3B2v7.51c GML4.3.1 ULTRAM : 704 Prod.Type:Com pp.1–11(col.fig.:NIL) ED:Ramesh PAGN: gopal SCAN: roopa

ARTICLE IN PRESS

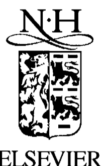

ELSEVIER

Available online at www.sciencedirect.com

SCIENCE DIRECT

Ultramicroscopy ■ (■■■■) ■■■–■■■

ultramicroscopy

www.elsevier.com/locate/ultramic

1 3 5 7 9 11 13 15 17 19 21 23 25 27 29 31 33 35 37 39 41 43 45 47

The differential reactivity of octahydridosilsesquioxane on Si(1 0 0)-2 × 1 and Si(1 1 1)-7 × 7: a comparative experimental study

Kevin S. Schneider[a], Kenneth T. Nicholson[a], Thomas M. Owens[a], Bradford G. Orr[b,c,1], Mark M. Banaszak Holl[a,c,*]

[a] Chemistry Department, University of Michigan, 930 N. University, 1500 Chemistry Building, Ann Arbor, MI 48109-1055, USA
[b] Physics Department, University of Michigan, Ann Arbor, MI 48109-1120, USA
[c] Applied Physics Program, University of Michigan, Ann Arbor, MI 48109-1120, USA

Received 29 May 2002; received in revised form 20 December 2002

Abstract

Scanning tunneling microscopy (STM), in conjunction with X-ray photoemission (XPS) and reflection-absorption infrared (RAIRS) spectroscopy, has been used to investigate the reaction of octahydridosilsesquioxane clusters ($H_8Si_8O_{12}$) on the Si(1 0 0)-2 × 1 and Si(1 1 1)-7 × 7 surfaces. The clusters exhibit a markedly different reactivity upon exposure to the two clean silicon surfaces. STM data is presented that, in conjunction with XPS and RAIRS data, provides numerous constraints upon possible geometries for the chemisorbed clusters. The sum of the data is consistent with a dissociative reaction mechanism on Si(1 0 0)-2 × 1, resulting in cluster attachment to the surface via a single vertex. Conversely, data of Si(1 1 1)-7 × 7 subject to a saturation exposure of $H_8Si_8O_{12}$ is presented that is highly suggestive of cluster decomposition on the surface.
© 2003 Published by Elsevier Science B.V.

PACS: 68.35.−p; 68.37.−d; 68.37.Ef; 68.55.Nq; 79.60.−i; 79.60.Dp; 79.60.Jv

Keywords: Si/SiO_2; Silicon–silicon oxide interface; Spherosiloxane; Hydridosilsesquioxane; Scanning tunneling microscopy X-ray photoemission spectroscopy; Reflection-absorption infrared spectroscopy

1. Introduction

49 51 53 55

Despite recent advances in bottom-up synthetic approaches to molecular-based logic and nanoelectronic devices (For a brief review of recent advances in molecular-based logic, see Ref. [1]), silicon-based logic gates are likely to remain as integral components to the electronics industry for at least the next two decades. The demand for

*Corresponding author. Chemistry Department, University of Michigan, 930 N. University, 1500 Chemistry Building, Ann Arbor, MI 48109-1055, USA. Tel.: +1-734-763-2283; fax: +1-734-936-2916.

E-mail addresses: orr@umich.edu (B.G. Orr), mbanasza@umich.edu (M.M. Banaszak Holl).

[1] Also Correspondence: Physics Department, University of Michigan, 500 E. University, 2477 Randall Labs, Ann Arbor, MI 48109-1120, USA.I

0304-3991/03/$ - see front matter © 2003 Published by Elsevier Science B.V.
doi:10.1016/S0304-3991(03)00028-7

UNCORRECTED PROOF

smaller, faster silicon-based metal-oxide-semiconductor field effect transistors (MOSFETs) necessitates the creation of thinner, more stable insulating silicon oxide (SiO_2) layers. Consequently, the oxidation of silicon remains one of the most important processes in the microelectronics industry [2]; however, a detailed understanding of the oxidation process and the structure of the resultant Si/SiO_2 interface remain elusive. Following Moore's Law (which states the number of transistors per area on integrated circuits doubles approximately every 18 months), SiO_2 insulating layers in functional MOSFET devices are expected to be <10 Å within the next 15 years. At these dimensions no "bulk" SiO_2 will remain as part of the insulating layer and electrical functionality will be dominated by the physical and chemical nature of the solid/solid interfaces that comprise the devices.

Numerous experimental [2–8] and theoretical [9–13] techniques have been employed to gain a better understanding of the oxidation process. The advent of the scanning tunneling microscope (STM) [14,15] has provided a heretofore-unattainable means to study the oxidation process at the atomic and molecular levels [16–20]. Despite this wealth of information, characterization of the oxidation process and the structure of the Si/SiO_2 interface remain controversial and poorly understood. In principle, the use of well-defined precursor molecules allows control of the structure of thin oxide films and provides self-limiting deposition conditions. Such studies can also yield benchmark chemical and spectroscopic data of ultrathin silicon oxide films and the Si/SiO_2 interfacial region.

The synthesis of model Si/SiO_2 interfaces have been achieved by the exposure of clean Si(1 0 0)-2×1 to gaseous hydridosilsesquioxane clusters [$(HSiO_{1.5})_n$; $n = 8, 10, 12, 14$] in ultrahigh vacuum (UHV) [21–26]. Hydridosilsesquioxane clusters are volatile, well-defined cage molecules with geometric dimensions equivalent to the ultrathin silicon oxide layers desired in future MOSFET devices. $H_8Si_8O_{12}$ is the smallest derivative of the hydridosilsesquioxane clusters and most commonly used in experimentation due to its relative ease of preparation and purification [27]. A cubic-shaped molecule, $H_8Si_8O_{12}$ has O_h symmetry and is comprised of silicon atoms at the cluster corners, oxygen atoms along cluster edges, and hydrogen atoms at the cluster corner vertices (Fig. 1).

Differing interpretations of X-ray photoemission (XPS) and reflection-absorption infrared (RAIRS) spectroscopic data have yielded two proposed bonding models of $H_8Si_8O_{12}$ chemisorbed to Si(1 0 0)-2×1: the "single vertex attachment" model [21,26] and the "cracked cluster" model (Fig. 2) [28]. The single vertex attachment model contains the following key propositions: (1) the cluster cage remains intact, (2) the cluster is activated at one of the Si–H vertices, and (3) the cluster bonds to a Si dimer atom via a single Si–Si bond (Fig. 2A). The cracked cluster model highlights Si–O bond scission along a cluster cage edge, resulting in a bridged bonding configuration across a Si dimer (Fig. 2B). Theoretical mechanistic studies by Raghavachari et al. modeling the reaction of $H_8Si_8O_{12}$ with a Si(1 0 0)-2×1 dimer suggest the single vertex attachment model is the thermodynamically favored product [28,29]. However, a larger calculated energy barrier along the reaction coordinate compared to that of the cracked cluster mechanism is believed to make the single vertex attachment product inaccessible. Therefore, the authors have concluded that the cracked cluster configuration would be the kinetically preferred product.

In this paper, results of comparative experimental studies of $H_8Si_8O_{12}$ chemisorbed on both the Si(1 0 0)-2×1 and Si(1 1 1)-7×7 surfaces are reported. XPS, RAIRS, and STM data are presented for both model Si/SiO_2 systems. The experimental data reveal profoundly different

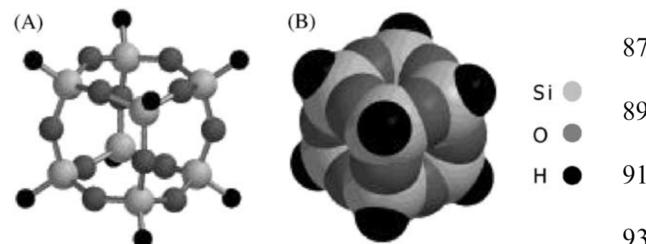

Fig. 1. $H_8Si_8O_{12}$: (A) Ball and stick model, (B) space filling model. Silicon, oxygen, and hydrogen atoms occupy cluster corners, edges, and corner vertices, respectively.

UNCORRECTED PROOF

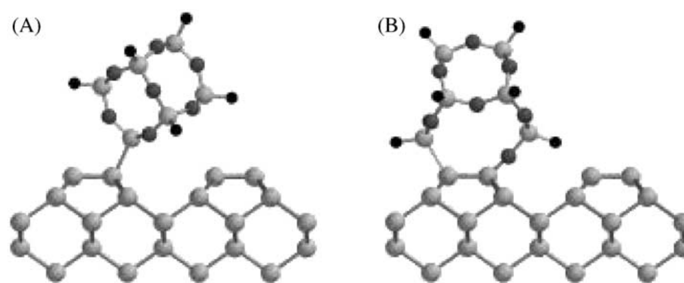

Fig. 2. Proposed bonding models for $H_8Si_8O_{12}$ chemisorbed to Si(1 0 0)-2 × 1: (A) Single vertex attachment model, (B) cracked cluster model.

reactivities for $H_8Si_8O_{12}$ adsorbates on the two Si surfaces. All three experimental techniques support a single vertex attachment model for $H_8Si_8O_{12}$ chemisorbed to Si(1 0 0)-2 × 1 in which the cluster cage remains intact following surface chemisorption. However, the data is consistent with $H_8Si_8O_{12}$ cluster decomposition on the Si(1 1 1)-7 × 7 surface. The data clearly display the apparent differences in the spectroscopic (XPS and RAIRS) and electronic/topographic (STM) signatures of intact and decomposed $H_8Si_8O_{12}$ clusters chemisorbed on Si. These results suggest a reappraisal of the mechanistic pathway put forth by Raghavachari et al. for reaction of $H_8Si_8O_{12}$ clusters on Si(1 0 0)-2 × 1 is necessary.

2. Experimental

Octahydridosilsesquioxane, $H_8Si_8O_{12}$, was synthesized from literature methods and sublimed twice [27]. Cluster purity was checked using ^{1}H NMR, IR, and gas chromatography-mass spectrometry (GC–MS). After loading the clusters into a glass or stainless steel UHV compatible sample container, the samples were further purified by sublimation via gentle heating in a water bath at ~323 K and prolonged exposure to pumping (>24 h) in UHV conditions. Clean Si(1 0 0) and/or Si(1 1 1) samples were exposed to 0.1 L to >1000 L (L = Langmuir = 1×10^{-6} Torr s) of gaseous $H_8Si_8O_{12}$ at typical dosing pressures of 4×10^{-8}–4×10^{-7} Torr.

Because silicon is highly transparent in the IR spectral region of interest, reflective buried-metal-layer Si(1 0 0) and Si(1 1 1) samples were used for RAIRS experiments [30].[2] Sample preparation procedures for RAIRS and XPS experiments have been explained elsewhere [24,31].

Soft-XPS experiments were performed at beamline U8B at the National Synchrotron Light Source (NSLS) at Brookhaven National Laboratory. An incident photon energy of 170 eV was used for the collection of Si 2p core-level and valence band spectra. The spectrometer and beamline have been previously described [4]. The RAIRS (Bio-Rad FTS-40 FTIR spectrometer) experimental apparatus has also been previously described [24]. Curve fitting was performed with Matlab v4.2c and either PHI-MAT v.4.0 or ESCA Tools v.4.2. Standard methods were employed for the deconvolution of the Si 2p spin orbit doublet in XPS core-level spectra [4].

Small (~3 mm × 7 mm × 0.25 mm) highly doped Si(1 0 0) and Si(1 1 1) samples for STM imaging experiments were cut from larger wafers (Virginia Semiconductor, Si(1 0 0): p-type, B-doped, resistivity ~0.003 Ω cm; Si(1 1 1): n-type, As-doped, resistivity ~0.001 Ω cm) and rinsed with acetone and methanol before being loaded into the UHV chamber. Samples were degassed at 873–973 K by resistive heating in UHV for at least 12 h (temperatures measured with a Minolta-Land infrared optical pyrometer; Cyclops 52, emissivity setting 0.7). Desorption of native oxide layers on degassed samples was accomplished by flashing to ~1400 K for 5–30 s followed by annealing at

[2] The buried-metal-layer samples were purchased from S. Mantl, Institute für Schicht–und Ionentechnik, Forschungszentrum Julich GmbH, P.O. Box 1913, 5170 Julich, Germany.

UNCORRECTED PROOF

~923 K for 30 s, yielding the commensurate Si(1 0 0)-2 × 1 and Si(1 1 1)-7 × 7 surface reconstructions with low defect densities. Prior to dosing with clusters, sample structures were assessed by STM.

STM images were acquired at room temperature in the constant-current mode using an RHK Technology, Inc. UHV300 Series variable temperature STM at typical sample biases (V_S) of −1 to −2 V and tunneling currents (I_T) of 0.5–2 nA. Commercially fabricated platinum/iridium (80/20) STM tips (Materials Analytical Services "Controlled Geometry" Pt/Ir STM tips) were used for imaging. Tip cleaning was accomplished through radiative heating by holding the tip directly above a Si sample (outside of tunneling range) heated to ~1023 K for 10–20 min prior to imaging. Image processing of STM constant current topographs consisted of plane and slope subtractions, image filters were not employed.

3. Results and interpretation

3.1. XPS data

The interaction of octahydridosilsesquioxane clusters with Si(1 0 0)-2 × 1 and Si(1 1 1)-7 × 7 has been experimentally investigated by XPS. The Si $2p_{3/2}$ core-level spectrum of a chemisorbed layer of $H_8Si_8O_{12}$ clusters on Si(1 0 0)-2 × 1 (Fig. 3A) is substantially different than for Si(1 1 1)-7 × 7 exposed to a saturating dose of $H_8Si_8O_{12}$ (Fig. 3B). Most obvious in Fig. 3A is the intensity in the region between 1 and 3 eV (shifts relative to bulk silicon set to a binding energy of 0 eV), not present in Fig. 3B. A mathematical least-squares decomposition of Fig. 3A into its constituent components suggests the spectrum is best fit as four features shifted 0.40, 1.04, 2.19, and 3.64 eV from the bulk Si feature (0.0 eV) having peak area ratios of approximately 1:1:1:7, respectively. The features are attributed to surface Si–H and Si–SiO_3 entities and cluster Si–SiO_3 and O_3Si–H entities, respectively, consistent with an intact cluster attached via a single vertex to a single Si surface dimer atom. From these chemical assignments, the peak area ratios associated with the attached cluster silicon

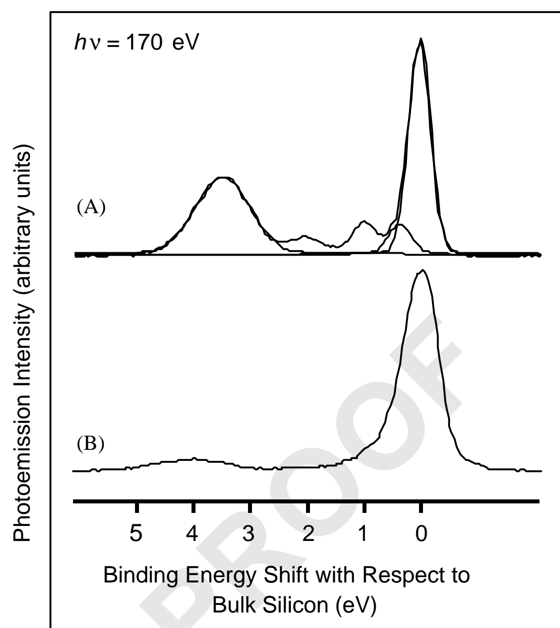

Fig. 3. Si $2p_{3/2}$ core-level spectra of Si samples following saturation exposure to $H_8Si_8O_{12}$: (A) Si(1 0 0)-2 × 1, (B) Si(1 1 1)-7 × 7.

vertex (Si–SiO_3) versus that of the unreacted cluster vertices (O_3Si–H) is in excellent agreement with the 1:7 ratio expected for a surface composed entirely of single vertex attached clusters. The Si $2p_{3/2}$ spectrum of Si(1 1 1)-7 × 7 subject to a saturation exposure to $H_8Si_8O_{12}$ (Fig. 3B) yields a single, broad peak at ~3.8 eV (shifted from bulk silicon) attributed to cluster-derived O_3Si–H entities. The significantly diminished signal intensity of cluster-derived O_3Si–H entities in Fig. 3B as compared to Fig. 3A indicates a substantially lower amount of $H_8Si_8O_{12}$ clusters have reacted with Si(1 1 1)-7 × 7 relative to Si(1 0 0)-2 × 1. No significant signal derived from an activated cluster vertex at 2.19 eV is apparent. For both Si(1 0 0)-2 × 1 and Si(1 1 1)-7 × 7, there is no evidence for the formation of chemi- or physisorbed cluster multilayers at room temperature (as one would expect predictable levels of attenuation in the photoemission intensities if multilayers had formed) [32]. In addition, the valence band spectrum (not shown) lacks numerous Si–H and Si–O derived features identified as arising from intact physisorbed and/or chemisorbed clusters. In

UNCORRECTED PROOF

conjunction with the valence band data, the absence of any features associated with an activated, intact cluster vertex suggests the cluster has decomposed on the Si(1 1 1)-7 × 7 surface, contrary to what is observed for reaction with Si(1 0 0)-2 × 1.

3.2. RAIRS data

RAIRS data (750–3000 cm^{-1}) has been collected for Si(1 0 0)-2 × 1 and Si(1 1 1)-7 × 7 samples subjected to saturation exposures of $H_8Si_8O_{12}$ (Fig. 4). The RAIRS spectrum of a chemisorbed layer of $H_8Si_8O_{12}$ clusters on Si(1 0 0)-2 × 1 displays intense features at 888, 1179, and 2271 cm^{-1} assigned as cluster-derived δ(Si–H), ν_a(Si–O), and ν(Si–H), respectively (Fig. 4B). These assignments are based on previous IR data obtained for $H_8Si_8O_{12}$ clusters [33,34], $H_8Si_8O_{12}$ chemisorbed on Si(1 0 0)-2 × 1 [24,31], $D_8Si_8O_{12}$ chemisorbed on Si(1 0 0)-2 × 1 [24], solution data of $RH_7Si_8O_{12}$ clusters [35], and density functional theory (DFT) calculations for $H_8Si_8O_{12}$ chemisorption to a model Si(1 0 0)-2 × 1 surface dimer [31,36]. Previous observation of the vibrational modes of the cluster framework at 414 and 576 cm^{-1} (not shown in Fig. 4) provide additional support for the chemisorption of intact clusters on the Si(1 0 0)-2 × 1 surface [37]. Calzaferri et al. have extensively discussed the origin and behavior of these cluster-derived breathing modes for both $H_8Si_8O_{12}$ and its single vertex substituted forms [38,39]. It is important to note the strong resemblance of Fig. 4B to solution IR spectra collected for $RH_7Si_8O_{12}$ monosubstituted clusters (not shown) [34,35]. Substitution of a single H atom results in a reduction of cluster symmetry from O_h to C_{3v}. Attachment of $H_8Si_8O_{12}$ clusters to the Si(1 0 0)-2 × 1 surface via a single vertex in which the cluster cage remains intact effectively lowers the cluster symmetry to C_{3v}. Therefore, the excellent overall agreement between Fig. 4B to solution IR spectra collected for $RH_7Si_8O_{12}$ clusters strongly supports the single vertex attachment model. When compared to Fig. 4B, the RAIRS spectrum of Si(1 1 1)-7 × 7 exposed to 700 L of $H_8Si_8O_{12}$ (Fig. 4A) contains noticeable differences. Fig. 4A shows intense features at approximately 884, 1104, 1164, and 2277 cm^{-1}. The features at 884 and 2277 cm^{-1} are assigned as cluster-derived δ(Si–H) and ν(Si–H), respectively. The large feature with splitting at 1104 and 1164 cm^{-1} is attributed to cluster-derived ν_a(Si–O).

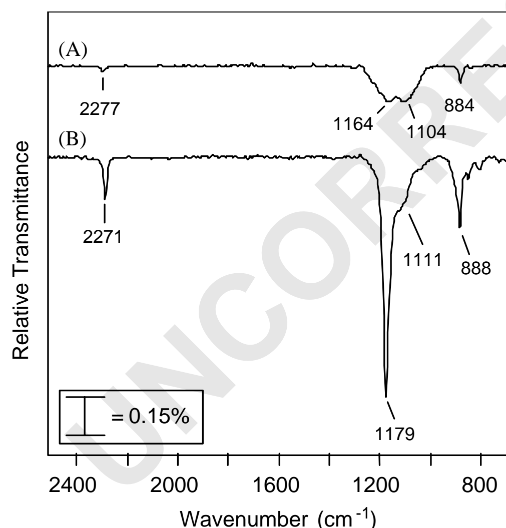

Fig. 4. (A) RAIRS (750–2500 cm^{-1}) of Si(1 1 1)-7 × 7 exposed to 700 L of $H_8Si_8O_{12}$, (B) RAIRS (750–2500 cm^{-1}) of a chemisorbed layer of $H_8Si_8O_{12}$ on Si(1 0 0)-2 × 1. Each spectrum represents (A) 800 and (B) 256 scans at 8 cm^{-1} resolution ratio to a clean Si background.

Comparison of the ν_a(Si–O) and ν(Si–H) regions yields some basic information concerning reactivity differences of $H_8Si_8O_{12}$ with Si(1 0 0)-2 × 1 and Si(1 1 1)-7 × 7. Most noticeably, the ν_a(Si–O) peak is much less intense for the Si(1 1 1)-7 × 7 sample than for the Si(1 0 0)-2 × 1 sample, suggesting a lower amount of cluster-derived oxide on Si(1 1 1)-7 × 7 than is observed for Si(1 0 0)-2 × 1, in good agreement with the XPS data. The ν_a(Si–O) peak is also much broader and displays a characteristic splitting for the Si(1 1 1)-7 × 7 sample unseen in the spectrum for a chemisorbed layer of $H_8Si_8O_{12}$ on Si(1 0 0)-2 × 1. Additionally, the relative intensities of the ν_a(Si–O) and ν(Si–H) regions are strikingly different. The ν(Si–H)/ν_a(Si–O) ratio for the Si(1 1 1)-7 × 7 sample exposed to a saturation dose of $H_8Si_8O_{12}$ (Fig. 4A) is ~0.03, whereas the ratio for a chemisorbed layer of closely packed clusters on Si(1 0 0)-2 × 1 (Fig. 4B) is ~0.06. A variety of factors can affect the observed intensities in RAIRS spectra, however, low coverages of intact

UNCORRECTED PROOF

$H_8Si_8O_{12}$ clusters chemisorbed to Si(1 0 0)-2 × 1 (not shown) share many similar features to Fig. 4A and give a ν(Si–H)/ν_a(Si–O) ratio of ~0.07. Although the comparison of the ν(Si–H)/ν_a(Si–O) ratios is not conclusive, it does suggest the $H_8Si_8O_{12}$ clusters have decomposed on Si(1 1 1)-7 × 7 losing some Si–H bonds in the process.

3.3. STM data

In an attempt to determine the nature of the bonding configuration of the $H_8Si_8O_{12}$ cluster and its relationship to the underlying Si(1 0 0)-2 × 1 and Si(1 1 1)-7 × 7 substrates, STM imaging experiments have been performed. The data presented herein display the electronic/topographic differences of intact and decomposed clusters on the Si surfaces as imaged by STM. To best view the registry of the chemisorbed clusters to the Si(1 0 0)-2 × 1 dimer rows, the $H_8Si_8O_{12}$ dose was limited to 0.1 L. A 350 Å × 350 Å filled states image displaying multiple clusters bound to three terraces on the Si(1 0 0)-2 × 1 surface is presented in Fig. 5A. In the image, the clusters appear as raised bundles of white dots, relative to the underlying Si(1 0 0)-2 × 1 substrate terrace. The clusters distribute about the terraces of the surface with no preference for bonding near step edges. No significant formation of cluster aggregate islands is apparent. The internal structure of the molecular cages, visible as four distinct bright dots roughly arranged in a square, is discernable in Fig. 5A. The image clearly displays a parallel orientation of the squares of dots with respect to the underlying Si(1 0 0)-2 × 1 dimer rows. Displayed in Fig. 5B is a 350 Å × 350 Å filled states image of the Si(1 1 1)-7 × 7 surface following exposure to a saturating dose of $H_8Si_8O_{12}$ clusters. The surface appears mottled with numerous bright protrusions. Additionally, atomic resolution of the Si(1 1 1)-7 × 7 sample surface is readily apparent in regions surrounding the surface protrusions, confirming the substantially lower reactivity of $H_8Si_8O_{12}$ clusters relative to the Si(1 0 0)-2 × 1 surface previously demonstrated by the XPS and RAIRS data. Statistical analyses of this image and several others reveal little preference for surface protrusion sites to particular regions of the Si(1 1 1)-7 × 7 unit cell. Unlike Fig. 5A, no internal molecular resolution is apparent in the surface protrusions present in Fig. 5B.

A 50 Å × 50 Å high-resolution filled states STM image of a single chemisorbed $H_8Si_8O_{12}$ cluster on Si(1 0 0)-2 × 1 is shown in Fig. 6A. The overall shape of the cluster is readily discernable, as is the internal structure of the molecular cage (visible as four distinct features forming a slightly skewed square). The cluster has an apparent height of approximately 0.6 Å and an apparent width of approximately 5 Å. Three key geometric attributes are apparent in this image: (1) the square formed by the four cluster features spans the dimer vacancy trench and overlaps two dimer rows, (2) the edges of this square are oriented parallel and perpendicular to the dimer row direction, and (3) there is a pronounced asymmetry in the brightness

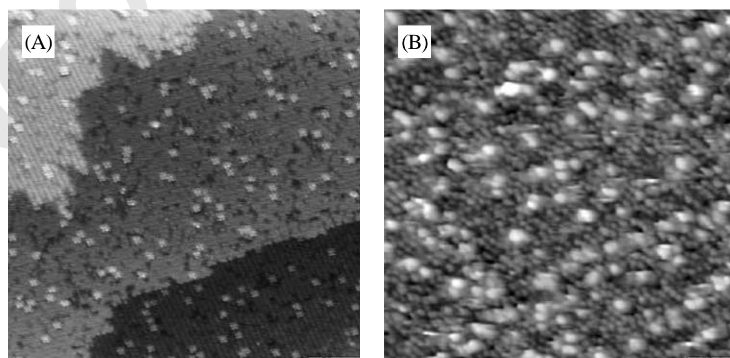

Fig. 5. 350 Å × 350 Å constant current, filled states STM topographs: (A) Si(1 0 0)-2 × 1 exposed to 0.1 L $H_8Si_8O_{12}$; $V_S = -1.50$ V, $I_T = 0.98$ nA, (B) Si(1 1 1)-7 × 7 exposed to 360 L $H_8Si_8O_{12}$; $V_S = -2.03$ V, $I_T = 0.55$ nA.

UNCORRECTED PROOF

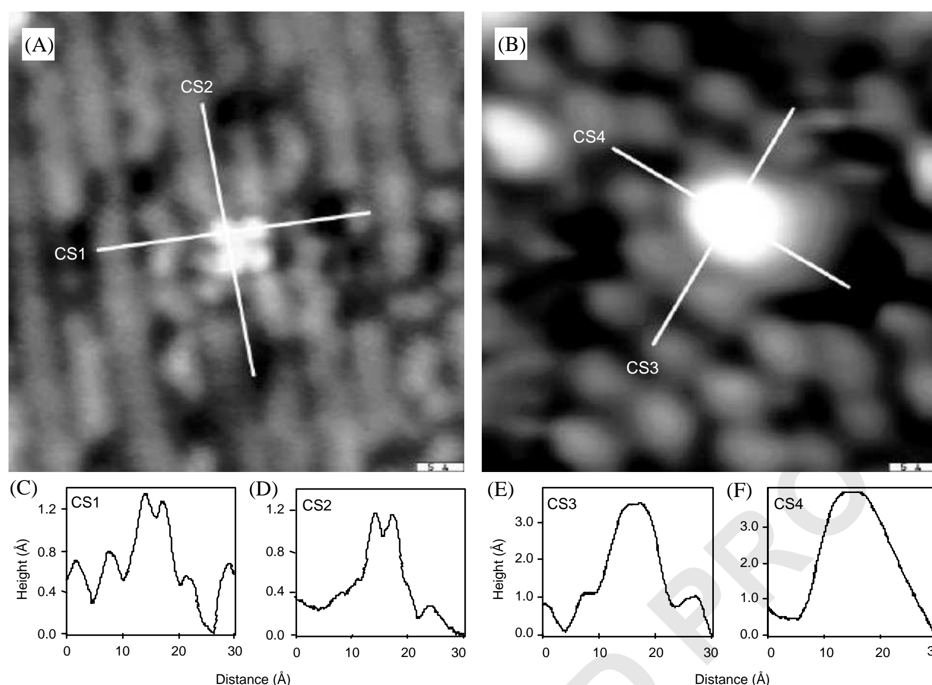

Fig. 6. 50 Å × 50 Å constant current, filled states STM topographs: (A) Si(1 0 0)-2 × 1 exposed to 0.1 L $H_8Si_8O_{12}$; $V_S = -1.50$ V, $I_T = 1.04$ nA, (B) Si(1 1 1)-7 × 7 exposed to 360 L $H_8Si_8O_{12}$; $V_S = -1.52$ V, $I_T = 2.31$ nA, (C)–(F) cross-sectional profiles displaying the apparent heights and widths (Å) of the corresponding cluster features in parts A and B.

of the pairs of cluster features that run parallel to the dimer rows. Cross-sectional analyses of the cluster features presented in Figs. 6C and D clearly highlight the asymmetry apparent in the pairs of cluster features (i.e. one pair of cluster features is noticeably larger in apparent height the other pair of cluster features). A 50 Å × 50 Å high-resolution filled states STM image of a single cluster-derived surface feature on Si(1 1 1)-7 × 7 is shown in Fig. 6B. The feature lacks the internal structure of the molecular cage visible in the chemisorbed cluster on Si(1 0 0)-2 × 1. Cross-sectional analyses of the surface feature (Fig. 6E and F) yield an apparent height of approximately 2.5 Å and an apparent width of approximately 15 Å. However, feature widths vary considerably amongst multiple images (typically ~5–15 Å), as evident in Fig. 5B.

To further elucidate the nature of the cluster bonding geometry to the Si(1 0 0)-2 × 1 surface, DFT calculations have been performed modeling the two proposed bonding geometries for a single $H_8Si_8O_{12}$ cluster chemisorbed to Si(1 0 0)-2 × 1. DFT calculations (pBP/DN) have been performed for a silyl-terminated cluster and for a cracked cluster bonded across a disilane molecule (mimicking a surface dimer) in order to produce electron density maps displaying the electrostatic potential of the cluster in both the single vertex and cracked cluster bonding configurations. The resulting electron density/electrostatic potential maps were overlaid on a large silicon slab according to their proposed bonding geometries. Fig. 7A and B represent the top-down views for a chemisorbed cluster according to the single vertex attachment and the cracked cluster models, respectively. On the clusters, areas of highest electrostatic potential are black and areas of lowest electrostatic potential are white; on the underlying Si slab, top-layer Si dimer atoms of the (2 × 1) reconstruction are black and bulk Si atoms are gray. Filled states STM images are derived from tunneling electrons out of the low-lying electronic states containing significant electron density near the Fermi energy with regions of highest electrostatic potential

UNCORRECTED PROOF

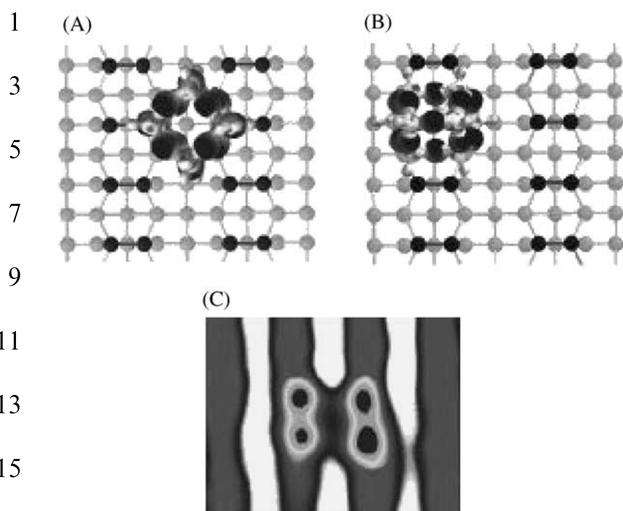

Fig. 7. (A) Top view of the electron density/electrostatic potential map of a silyl-terminated spherosiloxane cluster, $H_3Si–H_7Si_8O_{12}$, overlaid on a Si(1 0 0)-2 × 1 slab according to the single vertex attachment configuration. (B) Top view of the electron density map displaying the electrostatic potential of a cracked cluster bonded across a disilane molecule overlaid on a Si(1 0 0)-2 × 1 slab according to the cracked cluster attachment configuration. (C) A correlational filled states average STM image generated by averaging the signal from 30 individual $H_8Si_8O_{12}$ clusters in a 200 Å × 200 Å region.

recorded as height maxima. The DFT calculations indicate that the first four low-lying occupied states are localized on the cluster O atoms (the "lone pairs"). Taking this into account, it is possible to use Fig. 7A and B to predict the expected filled states STM images for both the single vertex attachment and the cracked cluster bonding configuration to the Si(1 0 0)-2 × 1 surface. Fig. 7A suggests a cluster with single vertex attachment imaged by STM would appear as four spots arranged in a square, situated between two Si dimer rows, and oriented parallel and perpendicular to the dimer row direction. Because the single vertex attachment model orients the cluster at an angle with respect to the Si(1 0 0)-2 × 1 surface (Fig. 2A), one pair of spots would appear slightly more intense than the other pair. Fig. 7B indicates a cracked cluster bonded to Si(1 0 0)-2 × 1 imaged by STM would appear as an intense bright spot, perhaps surrounded by a rectangle of four less intense spots, centered completely over one Si dimer row. Displayed in Fig. 7C is a correlational filled states average image generated by averaging the signal from 30 individual clusters in a 200 Å × 200 Å region. By averaging the signal of multiple clusters chemisorbed to the Si(1 0 0)-2 × 1 surface, Fig. 7C shows the features common to all individually bound clusters. The same three key geometric features previously identified for a single cluster in Fig. 6A are also apparent in Fig. 7C, demonstrating consistency of bonding geometry amongst multiple, individually bound clusters. Through comparison of Fig. 7C to Fig. 7A and B, it is readily apparent the filled states STM image of a $H_8Si_8O_{12}$ cluster chemisorbed to Si(1 0 0)-2 × 1 is consistent with all of the geometrical constraints put forth by the model for single vertex attachment. Conversely, the filled states STM image is not consistent with the geometrical attributes expected if the cracked cluster model were experimentally realized. Therefore, the STM data of $H_8Si_8O_{12}$ clusters chemisorbed to Si(1 0 0)-2 × 1 (Figs. 5A, 6A and 7C) provide strong evidence of intact clusters having single vertex attachment to the surface.

Unlike the chemisorption of $H_8Si_8O_{12}$ to Si(1 0 0)-2 × 1, STM images of Si(1 1 1)-7 × 7 dosed with $H_8Si_8O_{12}$ suggest cluster decomposition occurs following exposure to the surface. Recall, filled states STM images of chemisorbed $H_8Si_8O_{12}$ clusters on Si(1 0 0)-2 × 1 display internal resolution of the electronic states of individual, intact clusters. However, filled states STM images of Si(1 1 1)-7 × 7 exposed to $H_8Si_8O_{12}$ do not display the internal resolution characteristic of intact clusters. Furthermore, the apparent height of cluster-derived features is significantly higher on Si(1 1 1)-7 × 7 (~2.5 Å;Fig. 6E and F) than is observed on Si(1 0 0)-2 × 1 (~0.6 Å; Fig. 6C and D). This dramatically increased apparent height of cluster-derived features is likely the result of dangling bonds associated with decomposed clusters and/or the density of states associated with adsorbed cluster fragments. The variation in apparent widths of the surface protrusions in the STM data could result from adjacent or adjoining decomposed clusters or cluster fragments.

UNCORRECTED PROOF

4. Discussion

XPS, RAIRS, and STM data collected for the reaction of $H_8Si_8O_{12}$ clusters with the Si(1 0 0)-2 × 1 and Si(1 1 1)-7 × 7 surfaces have been presented. All three experimental techniques independently support cluster reaction with Si(1 0 0)-2 × 1 resulting in a chemisorbed layer comprised of intact, single vertex attached clusters as put forth by the bonding model in Fig. 2A. However, data from the three surface characterization techniques are consistent with a reaction involving cluster decomposition on the Si(1 1 1)-7 × 7 surface. Considering the controversy surrounding the bonding geometry of the cluster to the Si(1 0 0)-2 × 1 surface, the experimental results presented within this paper are significant. Based on theoretical calculations, Raghavachari et al. assert $H_8Si_8O_{12}$ bonds to Si(1 0 0)-2 × 1 according to a cracked cluster model that contends the cluster cage is broken following Si–O bond scission along a cluster edge (Fig. 2B) [28,29]. However, the experimental results display the differing spectroscopic (XPS and RAIRS) and electronic/topographic (STM) signatures of intact and decomposed $H_8Si_8O_{12}$ clusters chemisorbed on Si. Perhaps most convincingly, the STM data is entirely consistent with all three geometrical constraints put forth by the single vertex attachment model and is not at all consistent with the geometrical constraints required by the cracked cluster bonding configuration. Given these results, reaction of $H_8Si_8O_{12}$ with Si(1 0 0)-2 × 1 must proceed via a different mechanistic pathway than that proposed by Raghavachari et al. [28,29].

On the basis of transition state DFT calculations, Raghavachari et al. propose the reaction of $H_8Si_8O_{12}$ with Si(1 0 0)-2 × 1 proceeds via electrophilic attack of the buckled Si dimer with a cluster O atom. The dimer rows of the Si(1 0 0)-2 × 1 surface are believed to be slightly buckled, resulting in an unequal distribution of charge across the dimer Si–Si bond so that buckled-down Si atoms are electron deficient (tending to act as electrophiles) and the buckled-up atoms are electron rich (tending to act as nucleophiles). Raghavachari et al. suggest the reaction is initiated by the interaction of a cluster O atom with the buckled-down (electrophilic) surface dimer Si atom, analogous to that for the dissociation of water on Si(1 0 0)-2 × 1 [40]. For the purposes of these calculations, the commonly used dimer model, Si_9H_{12}, has been used to represent the Si(1 0 0)-2 × 1 surface. Whereas the Si_9H_{12} dimer model is typically an adequate surface representation for most calculations involving molecular adsorption to Si(1 0 0)-2 × 1, it is clearly not a sufficient substrate for modeling the adsorption of $H_8Si_8O_{12}$. Calculations involving the Si_9H_{12} slab inherently neglect the likely interactions (e.g. steric interference and/or electrostatic repulsion) of the surrounding substrate dimer rows. Some studies have probed the effects of intersite interactions by modeling two Si dimers within a row (using a larger $Si_{15}H_{16}$ slab as the model surface) [40], but to our knowledge no published reports exist examining potential interactions between dimer sites in different rows (as such a calculation would prove computationally taxing and expensive). Since the reaction of $H_8Si_8O_{12}$ with Si(1 0 0)-2 × 1 most likely does not proceed via electrophilic attack of a buckled-down dimer Si atom to a cluster O atom, we will now consider two other possible reaction mechanisms.

Electrophilic attack by a buckled-down dimer Si atom may also occur at a cluster H atom. Hydrogen atoms occur at cluster extremities (corner vertices), thus allowing for better molecular orbital overlap with a dimer Si atom while simultaneously minimizing potential extraneous cluster/surface repulsive interactions. Such a reaction is analogous to that observed for the dissociative adsorption of silane, SiH_4, on Si(1 0 0)-2 × 1 [41,42]. A reaction proceeding via this mechanistic pathway would yield a chemisorbed cluster attached via a single vertex, leaving the cluster cage intact, as predicted by the single vertex attachment model presented in Fig. 2A. This reaction mechanism has also been theoretically investigated by Raghavachari et al. and found to yield the thermodynamically favored reaction product (~0.5 eV more stable than that formed by breaking the Si–O bond, as proposed by the cracked cluster model) [28,29]. However, a larger energy barrier to the formation of Fig. 2A relative to the formation of the cracked cluster

UNCORRECTED PROOF

ULTRAM : 704
ARTICLE IN PRESS

(Fig. 2B) is predicted to make the single vertex attached cluster inaccessible. From the results presented in this paper, it is evident that the predictions provided by these electrophilic mechanisms are incorrect. The problem may arise from treating the cluster reaction mechanism as an acid/base reaction. Consideration of a number of synthetic studies investigating cluster reaction and functionalization can provide some additional insight [35,43–46]. An important class of reaction mechanism not expressly considered involves cluster Si–H radical abstraction.

There is precedent for the formation of a "cracked cluster" via electrophilic attack in the synthetic literature. Feher et al. have extensively studied the acid- and base-catalyzed cleavage and homologation of polyhedral oligosilsesquioxanes [44–46]. Succinctly, these studies have found that it is possible to selectively cleave one or more Si–O bonds in $R_8Si_8O_{12}$ clusters via reaction with strong acids (e.g. $HBF_4 \cdot OEt_2$–BF_3 or triflic acid) or strong bases (e.g. NEt_4OH) to cause cluster edge scission and yield incompletely condensed $R_7Si_7O_9(OH)_3$ molecules. In contrast to synthetic approaches that result in cluster edge cleavage, Calzaferri et al. and Klemperer et al. have utilized radical abstraction-based approaches for synthesizing completely and incompletely substituted $R_n'R_{8-n}Si_8O_{12}$ molecules that preserve the cluster cage integrity [35,43]. Considering that the results presented in this paper are consistent with $H_8Si_8O_{12}$ attachment to the surface via the single vertex model (preserving the cluster cage composition), a radical abstraction/radical trap mechanism provides the most likely reaction pathway. For the reaction of $H_8Si_8O_{12}$ with Si(1 0 0)-2 × 1, a surface Si–Si dimer should be construed as a reactive diradical (instead of a buckled, dimer dipole). A protruding Si dimer radical would be able to interact with an impinging cluster Si–H, abstracting a cluster H radical (•H) and simultaneously creating a cluster radical (•$H_7Si_8O_{12}$) in the process. The opposite Si dimer radical (2.35 Å separation distance), or even the Si radical present on an adjacent dimer within the row (3.85 Å separation distance), would then be available for a radical trap reaction with the cluster radical. This radical abstraction/radical trap reaction mechanism would yield an intact, chemisorbed cluster via a single vertex as put forth by Fig. 2A.

The preservation of the hydridosilsesquioxane cluster cage following reaction with the silicon surfaces may largely depend upon the proximity of surface diradicals. The Si(1 0 0)-2 × 1 surface contains Si dimers separated by 3.85 Å within a row, with Si dimer atom pairs (diradicals) 2.35 Å apart. However, nearest neighbor Si atoms of the Si(1 1 1)-7 × 7 surface (an adatom and rest atom) are separated by approximately 4 Å. Furthermore, the adatom layer is physically stacked atop the rest atom layer. The larger separation distance between nearest neighbor radical sites on the Si(1 1 1)-7 × 7 surface relative to the Si(1 0 0)-2 × 1 surface may inhibit a dissociative reaction involving radical abstraction and radical trap. Recall that many unreacted Si radical sites are present on the Si(1 1 1)-7 × 7 surface following exposure to a saturation cluster dose indicating that the monoradical sites on the surface are unable to directly abstract a hydrogen radical from the cluster. Additionally, because the rest atoms lie in the second layer relative to the adatom layer, steric hindrance may also prohibit a dissociative reaction of $H_8Si_8O_{12}$ with Si(1 1 1)-7 × 7. Consequently, unlike the reaction of $H_8Si_8O_{12}$ with Si(1 0 0)-2 × 1 in which intact clusters readily chemisorb to the surface via single vertices, $H_8Si_8O_{12}$ clusters are significantly less reactive with Si(1 1 1)-7 × 7 and those that do react with the surface undergo cluster decomposition.

Acknowledgements

Dow-Corning Corporation, RHK Technology, Inc. and the NSF (DMR-0093641 and DMR-9802586) are gratefully acknowledged for support of this work. M.M.B.H. is grateful for a Sloan Fellowship (1999–2002). K.S.S. thanks the NSF for an IGERT fellowship (DGE-9972776). Portions of this work were carried out at the National Synchrotron Light Source, Brookhaven National Laboratory, which is supported by the US Department of Energy (Division of Materials Science and Division of Chemical Sciences of the

UNCORRECTED PROOF

Office of Basic Energy Sciences) under Contract No. DE-AC02-98CH10886.

References

[1] R.F. Service, Science 294 (2001) 2442.
[2] H.Z. Massoud, E.H. Poindexter, C.R. Helms, The Physics and Chemistry of SiO_2 and the Si–SiO_2 Interface-3, The Electrochemical Society, Pennington, NJ, 1996.
[3] G. Hollinger, F.J. Himpsel, Phys. Rev. B 28 (1983) 3651.
[4] F.J. Himpsel, F.R. McFeely, A. Taleb-Ibrahimi, J.A. Yarmoff, G. Hollinger, Phys. Rev. B 38 (1988) 6084.
[5] J.R. Engstrom, D.J. Bonser, M.M. Nelson, T. Engel, Surf. Sci. 256 (1991) 317.
[6] T. Hattori, Crit. Rev. Solid State Mater. Sci. 20 (1995) 339.
[7] S. Iwata, A. Ishizaka, J. Appl. Phys. 79 (1996) 6653.
[8] F.J. Grunthaner, P.J. Grunthaner, Mater. Sci. Rep. 1 (1986) 65.
[9] W.A. Goddard, A. Redondo, T.C. McGill, Solid State Commun. 18 (1976) 981.
[10] M. Chen, I.P. Batra, C.R. Brundle, J. Vac. Sci. Technol. 16 (1979) 1216.
[11] S. Ciraci, S. Ellialtioglu, S. Erkoc, J. Vac. Sci. Technol. 21 (1982) 402.
[12] I.P. Batra, P.S. Bagus, K. Hermann, Phys. Rev. Lett. 52 (1984) 384.
[13] B. Schubert, P. Avouris, R. Hoffmann, J. Chem. Phys. 98 (1993) 7593.
[14] G. Binnig, H. Rohrer, C. Gerber, E. Weibel, Phys. Rev. Lett. 49 (1982) 57.
[15] G. Binnig, H. Rohrer, C. Gerber, E. Weibel, Phys. Rev. Lett. 50 (1983) 120.
[16] R.H. Koch, R.J. Hamers, Surf. Sci. 181 (1987) 333.
[17] F.M. Leibsle, A. Samsavar, T.-C. Chiang, Phys. Rev. B 38 (1988) 5780.
[18] J.P. Pelz, R.H. Koch, Phys. Rev. B 42 (1990) 3761.
[19] I.-W. Lyo, P. Avouris, B. Schubert, R. Hoffmann, J. Phys. Chem. 94 (1990) 4400.
[20] H. Tokumuto, K. Miki, H. Murakami, H. Bando, M. Ono, K. Kajimura, J. Vac. Sci. Technol. A 8 (1990) 255.
[21] M.M. Banaszak Holl, F.R. McFeely, Phys. Rev. Lett. 71 (1993) 2441.
[22] S. Lee, S. Makan, M.M. Banaszak Holl, F.R. McFeely, J. Am. Chem. Soc. 116 (1994) 11819.
[23] K.Z. Zhang, L.M. Meeuwenberg, M.M. Banaszak Holl, F.R. McFeely, Jpn. J. Appl. Phys. 36 (1997) 1622.
[24] J.N. Greeley, L.M. Meeuwenberg, M.M. Banaszak Holl, J. Am. Chem. Soc. 120 (1998) 7776.
[25] J.N. Greeley, M.M. Banaszak Holl, Inorg. Chem. 37 (1998) 6014.
[26] K.S. Schneider, Z. Zhang, M.M. Banaszak Holl, B.G. Orr, U.C. Pernisz, Phys. Rev. Lett. 85 (2000) 602.
[27] P.A. Agaskar, Inorg. Chem. 30 (1991) 2707.
[28] K. Raghavachari, J. Eng, J. Phys. Rev. Lett. 84 (2000) 935.
[29] K. Raghavachari, A. Pasquarello, J. Eng, M.S. Hybertson, Appl. Phys. Lett. 76 (2000) 3873.
[30] W. Ehrley, R. Butz, S. Mantl, Surf. Sci. 248 (1991) 193.
[31] J. Eng, K. Raghavachari, L.M. Struck, Y.J. Chabal, B.E. Bent, M.M. Banaszak Holl, F.R. McFeely, A.M. Michaels, G.W. Flynn, S.B. Christman, E.E. Chaban, G.P. Williams, K. Radermacher, S. Mantl, J. Chem. Phys. 108 (1998) 8680.
[32] K.Z. Zhang, J.N. Greeley, M.M. Banaszak Holl, F.R. McFeely, J. Appl. Phys. 82 (1997) 2298.
[33] M. Bartsch, P. Bornhauser, G. Calzaferri, R. Imhof, J. Phys. Chem. 98 (1994) 2817.
[34] G. Calzaferri, R. Imhof, K.W. Tornroos, J. Chem. Soc. Dalton Trans. (1994) 3123.
[35] C. Marcolli, G. Calzaferri, Appl. Organomet. Chem. 13 (1999) 213.
[36] K.T. Nicholson, M.M. Banaszak Holl, Phys. Rev. B 64 (2001) 155317.
[37] K.T. Nicholson, M.A. Biscotto, M.M. Banaszak Holl, Mater. Res. Soc. Symp. Proc. 567 (1999) 543.
[38] P. Bornhauser, G. Calzaferri, J. Phys. Chem. 100 (1996) 2035.
[39] C. Marcolli, G. Calzaferri, J. Phys. Chem. B 101 (1997) 4925.
[40] R. Konecny, D. Doren, J. Chem. Phys. 106 (1997) 2426.
[41] S.M. Gates, C.M. Greenlief, D.B. Breach, J. Chem. Phys. 93 (1990) 7493.
[42] A.R. Brown, D.J. Doren, J. Chem. Phys. 110 (1999) 2643.
[43] V.W. Day, W.G. Klemperer, V.V. Mainz, D.M. Millar, J. Am. Chem. Soc. 107 (1985) 8262.
[44] F.J. Feher, R. Terroba, J.W. Ziller, Chem. Commun. 22 (1999) 2309.
[45] F.J. Feher, K.D. Wyndham, D. Soulivong, F. Nguyen, J. Chem. Soc. Dalton Trans. 9 (1999) 1491.
[46] F.J. Feher, R. Terroba, J.W. Ziller, Chem. Commun. 21 (1999) 2153.

UNCORRECTED PROOF